MATERIALS CHEMISTRY FRONTIERS

CCS 中国化学会 CHINESE CHEMICAL SOCIETY

ICCAS

ROYAL SOCIETY OF CHEMISTRY

Cis- and Trans-orientation of Benzo[1,2-b:4,5-b']dithiophene-based Isomers in Organic Solar Cells

Journal:	*Materials Chemistry Frontiers*
Manuscript ID	QM-RES-10-2020-000778.R1
Article Type:	Research Article
Date Submitted by the Author:	03-Dec-2020
Complete List of Authors:	Lai, Hanjian; Southern University of Science and Technology, Chemistry Guo, Meigen; Shenzhen University, Chemistry Zhu, Yulin; Southern University of Science and Technology, Chemistry Chen, Lin; Southern University of Science and Technology, Chemistry Tan, Pu; Southern University of Science and Technology, Chemistry Yang, Chuluo; Shenzhen University, Chemistry He, Feng; Southern University of Science and Technology, Chemistry

ARTICLE

Cis- and Trans-orientation of Benzo[1,2-b:4,5-b′]dithiophene-based Isomers in Organic Solar Cells

Hanjian Lai, [‡a, b] Meigen Guo, [‡b, c] Yulin Zhu, [b] Lin Chen, [b] Pu Tan, [b] Chuluo Yang, [c] and Feng He*[b]

[a] School of Chemistry and Chemical Engineering, Harbin Institute of Technology, Harbin, 150001, China

[b] Shenzhen Grubbs Institute and Department of Chemistry, Southern University of Science and Technology, Shenzhen 518055, China

[c] Shenzhen Key Laboratory of Polymer Science and Technology College of Materials Science and Engineering, Shenzhen University, Shenzhen 518060, China

‡ These authors contributed equally

* E-mail: hef@sustech.edu.cn (F.H.)

Table of contents

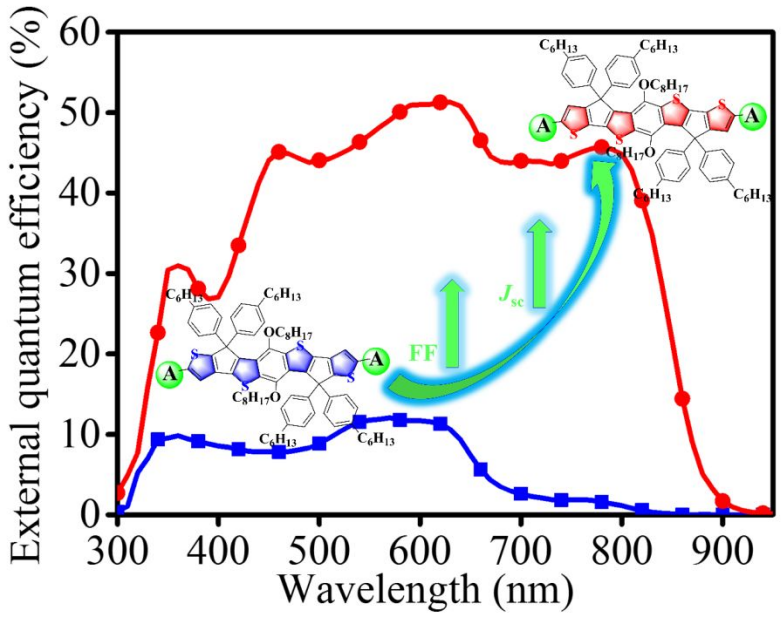

This work provides a new insight in the backbone configurations of A-D-A type non-fullerene acceptors. The two main isomers have significant differences in their optical and electric properties, resulting in a major impact on the current density and fill factor of the final organic solar cell devices.

Materials Chemistry Frontiers

Abstract

Significant breakthroughs have been achieved in bulk-heterojunction (BHJ)-based organic solar cells (OSCs) with power conversion efficiencies (PCE) of over 17% by the development of new cores of non-fullerene acceptors, and the isomers which are often produced in the synthesis of cores. Here, two BDT (benzo [1,2-b:4,5-b′]dithiophene)-based acceptors, which are isomers with different orientations of the thiophene rings on the backbone are reported. Different molecular configurations and electron cloud distribution of the isomers were developed by theoretical calculations, which indicate completely different optical properties and various electrochemical energy levels of the isomers. Grazing-incidence wide-angle X-ray scattering (GIWAXS) tests showed that the two isomers have different crystalline structures. The OSC devices developed from each of the two isomers exhibit significant differences in electron/hole mobilities and packing modes, leading to clearly distinct filling factors and short-circuit currents, affecting the PCEs of final devices. Our studies of core isomerism provide some new insights into the configurations of backbones and can assist the molecular design of new n-type electron acceptors.

Introduction

As progressive and promising renewable energy technology, OSCs have attracted extensive attention due to their advantages in light-weight, low-cost fabrication, flexibility and large area, which are valuable in building integration, portable electronics and photovoltaic power plants.[1-5] The photoactive layer is considered to be the key component of the BHJ-based OSC structure, which usually contains a p-type electron donor and an n-type electron acceptor. The state-of-the-art acceptors are categorized as fullerene-based or non-fullerene-based acceptors (NFA).[6-9] In 2015, Zhan et al. reported an A-D-A-type molecule ITIC based on an indacenobis(dithieno[3,2-b;2′,3′-d]thiophene) core,[10] which broke a twenty year monopoly of fullerene-based materials,[11-14] and extended the PCEs rapidly to 14%.[15-18] More recently, Zou's group reported a more promising molecule named Y6, which is an A-DAD-A-type acceptor based on a (dithienothiophen[3,2-b]-pyrrolobenzothiadiazole) fused core.[19] The PCEs based on this type of acceptor have surpassed 17% due to its excellent spectral absorption and lower energy loss.[20-24] Design and synthesis of new cores is an effective strategy with which to promote the development of OSCs.

Isomers are often produced in the synthesis of new cores however, resulting in different physical and chemical properties which further influence the performance of OSC devices.[25, 26] For example, as shown in **Figure 1**, Chen et al. reported two isomeric core-based acceptors FTCT-FIC and FCTT-FIC, [27] in which the distances between side-chains and terminal groups are 10.52 Å for FTCT-FIC and 12.21 Å for FCTT-FIC. Although a shorter separation should lead to formation of more ideal J-aggregation, obtaining red-shifted absorption, the intermolecular packing on two terminal sides would be hindered in a way that would inhibit charge transfer. An FCTT-FIC with larger separation will exhibit a PCE higher than

12.23% with better and more balanced mobilities. Zhan's group proved this by studying the relationship between the position of thiophene rings and the performance of OSC devices.[28] Similar results are found in ITIC and NFBDT systems.[10, 29] These results demonstrate that the different positions of thiophene rings in the cores have a significant effect on the molecular properties and devices based on the cores. However, while comparison of isomers with thiophene rings in different positions has been achieved, the effect of the orientation of thiophene rings has been rarely studied.

Two BDT (benzo[1,2-b:4,5-b′]dithiophene)-based acceptors, **BDT$_t$IC-*γ*Cl** and **BDT$_c$IC-*γ*Cl** have been designed and synthesized. They differ in the orientation of thiophene rings on the backbone, which can be seen as trans-oriented and cis-oriented[30], respectively. Interestingly, the properties of the two isomers and their derived OSC devices differ significantly. Theoretical calculations show that higher dipole moments (μ_m) were found in **BDT$_c$IC-*γ*Cl**, and this supports better intermolecular charge transfer for superior FF.[31,32] More importantly, the HOMO and the LUMO of **BDT$_t$IC-*γ*Cl** are localized on an electron-rich backbone and on electron-withdrawing terminal groups respectively, and this leads to a typical strong charge transfer (CT)-like character with broad symmetrical 'camel-back' absorption.[33-35] **BDT$_c$IC-*γ*Cl** on the other hand shows a more red-shifted sharp peak absorption due to the large overlap of its LUMO and HOMO wavefunctions, which enhances the oscillator strength of the HOMO →LUMO transition, and is good for utilization of photons.[33] The TD-DFT (B3LYP/6-31G*) calculation values were consistent with the above results. Consequently, a much higher short-circuit current (J_{sc}) of 13.77 mA cm^{-2} was achieved by **BDT$_c$IC-*γ*Cl**-based OSC devices which is consistent with the J_{cal} of 13.62 mA cm^{-2} observed in an external quantum efficiency (EQE) test. Additionally, **BDT$_c$IC-*γ*Cl**-based devices possess larger electron/hole mobilities of 4.2×10^{-5} and 5.6×10^{-5} cm^2 V^{-1} s^{-1} and a more balanced hole/electron ratio of

1.3, leading to a higher fill factor (FF) of 62.25%. On the other hand, a grazing-incidence wide-angle X-ray scattering (GIWAXS) test indicates that more regular and ordered crystalline structures exist in neat **BDT$_c$IC-*γ*Cl** and its blend films due to the greater number of signal peaks and the higher crystal coherence length (CCL), [36, 37] which is consistent with higher *J*sc and FF values. Our results demonstrate that the isomerism resulting from the orientation of thiophene rings on the backbone have a considerable influence on the distribution of electron cloud, the optical properties and molecular packing, thereby further affecting the performance of the OSC devices. This study of core isomerism could provide some guidance for molecular design and development of new n-type electron acceptors.

Result and Discussion

BDT$_t$IC-*γ*Cl and **BDT$_c$IC-*γ*Cl** were synthesized by a Knoevenagel condensation reaction between BDT-based cores and an IC-Cl-*γ* end group,[38, 39] as shown in **Figure 2**, where the IC-Cl-*γ* was obtained by recrystallization from IC-Cl-*m*.[40, 41] The two BDT-based cores were synthesized by previously published cyclization reactions.[42, 43] They are isomers but differ in the orientation of the thiophene ring on the two sides of the core, one is cis-oriented and the other is trans-oriented. The synthetic routes are shown in **Scheme 1** and further synthesis details are provided in the Supporting Information (SI). **Figure S1** and **Figure S2** show the thermogravimetric analysis (TGA) and differential scanning calorimetry (DSC) results analyzing the thermal properties of **BDT$_t$IC-*γ*Cl** and **BDT$_c$IC-*γ*Cl**. It was found both of these compounds meet the thermal requirements for device processing and in addition, they exhibit good solubility in dichloromethane, chloroform, toluene and chlorobenzene, which can be used for solution

processing. The commonly used PBDB-TF (PM6) was chosen as a polymer donor to match with the two acceptors as an active layer of OSCs, the chemical structure of PBDB-TF was shown in **Scheme S2**.

The differences of molecular configurations and electronic distributions between **BDT$_t$IC-*γ*Cl** and **BDT$_c$IC-*γ*Cl** were studied by the density functional theory (DFT) method of RB3LYP 6-31G (d, p). As shown in **Figure 2**, both of the acceptors have a linear structure with an S-O=C interlock configuration.[44, 45] Good molecular coplanarity with dihedral angles of 0.12^o /0.33^o for **BDT$_t$IC-*γ*Cl** and 0.07^o /0.07^o for **BDT$_c$IC-*γ*Cl** between terminal groups and cores were observed. The four phenylcycloalkane side chains are sp^3 hybridized on either side of the core, which hinders the packing between the cores and leads to J-aggregation by π-π stacking between terminal groups.[41] The calculated dipole moment (μ_m) of **BDT$_t$IC-*γ*Cl** is 0.15 D and that of **BDT$_c$IC-*γ*Cl** is 1.01 D. The higher μ_m of **BDT$_c$IC-*γ*Cl** would support its obtaining better intermolecular charge transfer, leading to a superior FF.[46] More importantly, **BDT$_t$IC-*γ*Cl** and **BDT$_c$IC-*γ*Cl** show obvious differences in the electronic cloud distribution. As shown in **Figure 3**, the HOMO and the LUMO of **BDT$_t$IC-*γ*Cl** are localized on the electron-rich backbone and electron-withdrawing terminal groups, respectively, while **BDT$_c$IC-*γ*Cl** possesses more delocalized LUMO and HOMO wavefunctions, resulting in a large overlap between them. The calculated LUMO and HOMO energy level values are -3.28 eV and -5.34 eV for **BDT$_t$IC-*γ*Cl**, and -3.45 eV and -5.40 eV for **BDT$_c$IC-*γ*Cl**, respectively.

The optical properties of **BDT$_t$IC-*γ*Cl** and **BDT$_c$IC-*γ*Cl** were determined by UV-Vis absorption. The two isomers display completely different absorption properties. As shown in **Figure 4a**, a typical symmetrical ‘camel-back’ solution absorption with a blue-shifted peak value of 480 nm and a red-shifted peak value of 645 nm was found for **BDT$_t$IC-*γ*Cl**. The reason for this lies in its localized LUMO and

HOMO wavefunctions, leading to a typical strong charge transfer (CT)-like character with broad absorption. The red-shifted peak represents a localized transition to a CT state and the blue-shifted peak is ascribed to a delocalized excitonic π-π* transition.[33, 34] On the contrary, **BDT$_c$IC-*γ*Cl** shows a more red-shifted sharp peak absorption at 743 nm because of a large overlap of the LUMO and HOMO wavefunctions. Consequently, the oscillator strength of the HOMO to LUMO transition should be enhanced by this delocalized electronic cloud distribution.[33-35] **Figure 4b** shows the absorption in solid state; maximum absorption peaks at 678 nm and at 791 nm were shown by **BDT$_t$IC-*γ*Cl** and **BDT$_c$IC-*γ*Cl**, respectively. The red-shifted absorptions from solution to film were identified with the J-aggregation behaviors of the two isomers. The red-shifted absorption and higher extinction coefficients (1.33×10^5 L mol^{-1} cm^{-1}) of **BDT$_c$IC-*γ*Cl** would help enhance utilization of photons to obtain a higher current density. This result indicates that the isomerization of cores has a considerable influence on the optical properties.

To further understand the absorption characteristics of two isomers, the TD-DFT (B3LYP/6-31G*) calculations was used to investigate the oscillator strengths and simulated excitation energies of them. As shown in **Figure S3** and **Figure S4**, three different excited states were found in both **BDT$_t$IC-*γ*Cl** and **BDT$_c$IC-*γ*Cl**, where the **BDT$_t$IC-*γ*Cl** exhibit blue-shifted excitation energies of 720.2, 702.9, 548.0 nm with oscillator strengths of 0.473, 0.002, and 0.073, respectively, while the excitation energies of 753.3, 626.2, 550.4 nm with corresponding oscillator strengths of 2.139, 0.004, and 0.135 were found in **BDT$_c$IC-*γ*Cl**. As a result, the red-shifted excitation energy of **BDT$_c$IC-*γ*Cl** by theoretical calculation is consistent with the experimental data from **Figure 4a**, and the higher oscillator strength of **BDT$_c$IC-*γ*Cl** agrees well with the delocalized electronic cloud distribution of it. The electrochemical energy levels of

two isomers determined by the CV method are shown in **Figure 4c**, where the oxidation-reduction potential of **BDT$_t$IC-γCl** and **BDT$_c$IC-γCl** are 0.75/-0.57 eV and 0.83/-0.45 eV (refer to ferrocene/ferrocenium redox couple), respectively, and the corresponding HOMO and LUMO energy levels are -5.21/-3.89 eV and -5.29/-4.01 eV, respectively, which are shown in **Figure 4d**. This trend of energy level variation is consistent with the results of theoretical calculations.

OSC devices were fabricated to compare the photovoltaic performance of **BDT$_t$IC-γCl** with that of **BDT$_c$IC-γCl**[40, 46, 49, 50]. **Figure 5a** shows the J-V curves of the two isomers. It was found a V_{oc} of 0.89 V, a J_{sc} of 13.77 mA cm^{-2}, and an FF of 62.25% was achieved by **BDT$_c$IC-γCl**, while **BDT$_t$IC-γCl** exhibited a lower V_{oc} of 0.81 V, a J_{sc} of 2.26 mA cm^{-2}, and an FF of 39.06%. The red-shifted absorption and higher extinction coefficients of **BDT$_c$IC-γCl**-based devices are an important reason for the higher current density. **Figure 5b** shows the EQE curves of **BDT$_t$IC-γCl**- and **BDT$_c$IC-γCl**-based devices. The corresponding calculated J_{cal} values are 2.02 mA cm^{-2} and 13.62 mA cm^{-2}, respectively, which is consistent with the results from the J-V test. On the other hand, the carrier transport properties of the trans- and cis-acceptors were determined by an SCLC test, as shown in **Figures 5c** and **5d**. The **BDT$_c$IC-γCl**-based devices have an electron mobility and a hole mobility of 4.2×10^{-5} and 5.6×10^{-5} cm^2 V^{-1} s^{-1} respectively, while a lower electron mobility of 4.6×10^{-6} and a hole mobility of 7.5×10^{-6} cm^2 V^{-1} s^{-1} was found for **BDT$_t$IC-γCl**, and would lead to a disadvantage in the current density. Furthermore, with the inferior hole mobility, an electron ratio of 1.6 for **BDT$_t$IC-γCl** would lead to a lower FF. Those results show that the core isomerism has a major influence on the charge transport properties and further affects the performance of OSC devices.

Figure S5 depicts the atomic force microscopy (AFM) and transmission electron microscopy (TEM) test results of two isomeric acceptor-based films. It was found from TEM images that both **BDT$_t$IC-*γ*Cl** and **BDT$_c$IC-*γ*Cl** have obvious fibrillar networks and possess smooth and uniform morphology with similar root mean square (RMS) deviations of 1.54 and 1.47 nm from the AFM measurements, respectively. [47] The corresponding 3D AFM images are shown in **Figures S3c** and **S3f**. The results suggest that the isomerism of the cores has little effect on the film morphologies.

To further visualize the isomer effects on the molecular packing in the solid state, the GIWAXS was conducted on **BDT$_t$IC-*γ*Cl** and **BDT$_c$IC-*γ*Cl** neat and blend films. As depicted in **Figure 6**, the 2D GIWAXS images exhibit strong intensities in the q_z direction, indicating that a dominant face-on orientation exists, in which the (010) scattering peaks in the out of plane (OOP) direction are 1.72 and 1.70 Å^{-1} for **BDT$_t$IC-*γ*Cl** and **BDT$_c$IC-*γ*Cl** neat films, respectively. These change to 1.69 and 1.67 Å^{-1} after blending with polymer donor, which corresponds to a negligible difference in the π-π distances of 3.65/3.69 Å for neat films and 3.72/3.76 Å for blend films, respectively. This result demonstrates that isomeric cores have negligible influence on intermolecular packing, which is consistent with the previous studies that show that the intermolecular interactions are mainly determined by terminal groups and form regular J-aggregates.[40, 48] However, some differences could be found in the in-plane (IP) direction. In detail, the **BDT$_t$IC-*γ*Cl** neat film exhibits a strong intensity at 0.30 Å^{-1} in the IP direction with a full-width at half maximum (FWHM) of 0.17 Å^{-1}, corresponding to a (100) lamellar distance of 20.93 Å. The crystal coherence length (CCL) along this direction is 36.94 Å, while two bands at 0.30 Å^{-1} and 0.40 Å^{-1} were found in the IP for the **BDT$_c$IC-*γ*Cl** neat film, corresponding to the (100) and (001) lamellar distances of 20.93 Å and 15.7 Å. The matching CCL of (100) is 62.82 Å. More signal peaks and higher

CCLs, indicating more regular and ordered crystalline structures exist in **BDT$_c$IC-γCl**, [37] and would support high charge mobilities. The same relationship was found in two blend films, implying that higher *J*sc and FF would be realized in the **BDT$_c$IC-γCl**-based devices. Those results demonstrate that isomerism of cores can affect the molecular packing in the IP direction but to some extent, fails to influence the intermolecular stacking in the OPP direction.

Conclusions

Two isomers **BDT$_t$IC-γCl** and **BDT$_c$IC-γCl** have been synthesized and used to compare the isomerism effect caused by the orientation of thiophene rings on the backbone. The properties of the two isomers and their OSC devices were found to be significantly different. The HOMO and the LUMO of **BDT$_t$IC-γCl** are localized on the electron-rich backbone and electron-withdrawing terminal groups while **BDT$_c$IC-γCl** shows more delocalized LUMO and HOMO wavefunctions resulting in a large overlap between them, leading to a more red-shifted sharp peak absorption in **BDT$_c$IC-γCl** and a typical symmetrical 'camel-back' absorption in **BDT$_t$IC-γCl**. This is also proved by TD-DFT (B3LYP/6-31G*) calculation. Consequently, a PCE of 7.61% with V_{oc} of 0.89 V, J_{sc} of 13.77 mA cm^{-2} and FF of 62.25% was achieved by **BDT$_c$IC-γCl**-based OSCs, which is a large improvement from the PCE of 0.71% produced by the **BDT$_t$IC-γCl**-based OSC. The GIWAXS test indicates that more regular and ordered crystalline structures exist in **BDT$_c$IC-γCl** neat and blend films, which is consistent with its larger electron and hole mobilities and a more balanced hole/electron ratio of 1.3, resulting in better photoresponse current by EQE and a higher FF. Our studies of core isomerization could avoid some design failure and enhance understanding of the core design in high-performance non-fullerene acceptors.

Conflicts of interest

There are no conflicts to declare.

Acknowledgements

This work was financially supported by the National Natural Science Foundation of China (21975115, 21733005, 51773087, 51903116), Shenzhen Fundamental Research Program (JCYJ20180302180238419, and KQJSCX20180319114442157) and Shenzhen Nobel Prize Scientists Laboratory Project (C17213101), Guangdong Provincial Key Laboratory of Catalysis (2020B121201002), Guangdong Innovative and Entrepreneurial Research Team Program (2016ZT06G587) and Shenzhen Sci-Tech Fund (KYTDPT20181011104007). We thank Dr. Joseph Strzalka and Dr. Zhang Jiang for the assistance with GIWAXS measurements. Use of the Advanced Photon Source (APS) at the Argonne National Laboratory was supported by the U.S. Department of Energy, Office of Science, Office of Basic Energy Sciences, under contract No. DE-AC02-06CH11357. We also thank the SUSTech Core Research Facilities for the AFM and TEM measurements.

Notes and references

1. Y. Li, G. Xu, C. Cui and Y. Li, Flexible and semitransparent organic solar cells, *Adv. Energy Mater.*, 2017, **8**, 1701791.
2. S. Dai and X. Zhan, Nonfullerene acceptors for semitransparent organic solar cells, *Adv. Energy Mater.*, 2018, **8**, 1800002.
3. K. Fukuda, K. Yu and T. Someya, The future of flexible organic solar cells, *Adv. Energy Mater.*, 2020, **10**, 2000765.
4. G. Li, R. Zhu and Y. Yang, Polymer solar cells, *Nat. Photonics*, 2012, **6**, 153-161.
5. A. J. Heeger, 25th anniversary article: bulk heterojunction solar cells: understanding the mechanism of operation, *Adv. Mater*., 2014, **26**, 10-28.
6. P. Meredith, W. Li and A. Armin, Nonfullerene Acceptors: a renaissance in organic photovoltaics?, *Adv. Energy Mater.*, 2020, **10**, 2001788.
7. J. Chen, Y. Chen, L. Feng, C. Gu, G. Li, N. Su, G. Wang, S. Swick, W. Huang, X. Guo, A. Facchetti and T. J. Marks, Hole (donor) and electron (acceptor) transporting organic semiconductors for bulk-heterojunction solar cells, *EnergyChem*, 2020, **2**, 100042.
8. X. Wan, C. Li, M. Zhang and Y. Chen, Acceptor–donor–acceptor type molecules for high performance organic photovoltaics–chemistry and mechanism, *Chem. Soc. Rev.,* 2020, **49**, 2828.
9. E. M. Speller, A. J. Clarke, J. Luke, H. K. H. Lee, J. R. Durrant, N. Li, T. Wang, H. C. Wong, J.-S. Kim, W. C. Tsoi and Z. Li, From fullerene acceptors to non-fullerene acceptors: prospects and

challenges in the stability of organic solar cells, *J. Mater. Chem. A,* 2019, **7**, 23361.

10. Y. Lin, J. Wang, Z. Zhang, H. Bai, F. Li, D. Zhu and X. Zhan, An Electron Acceptor Challenging Fullerenes for Efficient Polymer Solar Cells, *Adv. Mater*., 2015, **27**, 1170-1174.
11. X. Ouyang, R. Peng, L. Ai, X. Zhang and Z. Ge, Efficient polymer solar cells employing a non-conjugated small-molecule electrolyte, *Nat. Photonics*, 2015, **9**, 520-524.
12. Y. Liu, J. Zhao, Z. Li, C. Mu, W. Ma, H. Hu, K. Jiang, H. Lin, H. Ade and H. Yan, Aggregation and morphology control enables multiple cases of high-efficiency polymer solar cells, *Nat. Commun*., 2014, **5**, 5293.
13. J. Zhao, Y. Li, G. Yang, K. Jiang, H. Lin, H. Ade, W. Ma and H. Yan, Efficient organic solar cells processed from hydrocarbon solvents, *Nat. Energy*, 2016, **1**, 15027.
14. Z. He, B. Xiao, F. Liu, H. Wu, Y. Yang, S. Xiao, C. Wang, T. P. Russell and Y. Cao, Single-junction polymer solar cells with high efficiency and photovoltage, *Nat. Photonics*, 2015, **9**, 174-179.
15. H. Yao, Y. Cui, D. Qian, C. S. Ponseca, Jr., A. Honarfar, Y. Xu, J. Xin, Z. Chen, L. Hong, B. Gao, R. Yu, Y. Zu, W. Ma, P. Chabera, T. Pullerits, A. Yartsev, F. Gao and J. Hou, 14.7% efficiency organic photovoltaic cells enabled by active materials with a large electrostatic potential difference, *J. Am. Chem. Soc*, 2019, **141**, 7743-7750.
16. L. Yang, Z. Hu, Z. Zhang, J. Cao, H. Wang, J. Yu, F. Zhang and W. Tang, Molecular engineering of acceptors to control aggregation for optimized nonfullerene solar cells, *J. Mater. Chem. A*, 2020, **8**, 5458-5466.
17. Z. Zhang, L. Yang, Z. Hu, J. Yu, X. Liu, H. Wang, J. Cao, F. Zhang and W. Tang, Charge density modulation on asymmetric fused-ring acceptors for high-efficiency photovoltaic solar cells, *Mater. Chem. Front.*, 2020, **4**, 1747-1755.

18. Y. Ma, D. Cai, S. Wan, P. Yin, P. Wang, W. Lin, Q. Zheng, Control over π-π stacking of heteroheptacene-based nonfullerene acceptors for 16% efficiency polymer solar cells, *Natl. Sci. Rev.*, 2020, https://doi.org/10.1093/nsr/nwaa189.

19. J. Yuan, Y. Zhang, L. Zhou, G. Zhang, H.-L. Yip, T.-K. Lau, X. Lu, C. Zhu, H. Peng, P. A. Johnson, M. Leclerc, Y. Cao, J. Ulanski, Y. Li and Y. Zou, Single-junction organic solar cell with over 15% efficiency using fused-ring acceptor with electron-deficient core, *Joule*, 2019, **3**, 1140-1151.

20. Y. Cui, H. Yao, J. Zhang, K. Xian, T. Zhang, L. Hong, Y. Wang, Y. Xu, K. Ma, C. An, C. He, Z. Wei, F. Gao and J. Hou, Single-junction organic photovoltaic cells with approaching 18% efficiency, *Adv. Mater.*, 2020, **32**, 1908205.

21. H. Lai and F. He, Crystal Engineering in Organic Photovoltaic Acceptors: A 3D Network Approach, *Adv. Energy Mater*., 2020, 202002678.

22. Q. Liu, Y. Jiang, K. Jin, J. Qin, J. Xu, W. Li, J. Xiong, J. Liu, Z. Xiao, K. Sun, S. Yang, X. Zhang and L. Ding, 18% efficiency organic solar cells, *Sci. Bull*., 2020, **65**, 272-275.

23. X. Xu, L. Yu, H. Yan, R. Li and Q. Peng, Highly efficient non-fullerene organic solar cells enabled by a delayed processing method using a non-halogenated solvent, *Energy Environ. Sci.*, 2020, doi.org/10.1039/D0EE02034F.

24. S. Li, C.-Z. Li, M. Shi and H. Chen, New phase for organic solar cell research: emergence of y-series electron acceptors and their perspectives, *ACS Energy Lett.*, 2020, **5**, 1554-1567.

25. Z. Zhou, J. Duan, L. Ye, G. Wang, B. Zhao, S. Tan, P. Shen, H. Ryu, H. Y. Woo and Y. Sun, Simultaneously improving the photovoltaic parameters of organic solar cells via isomerization of benzo[b]benzo[4,5]thieno[2,3-d]thiophene-based octacyclic non-fullerene acceptors, *J. Mater. Chem. A,* 2020, **8**, 9684-9692.

26. J. Wang, J. Zhang, Y. Xiao, T. Xiao, R. Zhu, C. Yan, Y. Fu, G. Lu, X. Lu, S. R. Marder and X. Zhan, Effect of isomerization on high-performance nonfullerene electron acceptors, *J. Am. Chem. Soc,* 2018, **140**, 9140–9147.

27. Y. Xue, F. Cao, P. Huang, Y. Su and Y. Cheng, Isomeric effect of fluorene-based fused-ring electron acceptors to achieve high-efficiency organic solar cells, *J. Mater. Chem. A*, 2020, **8**, 5315-5322.

28. G. Cai, J. Zhu, Y. Xiao, M. Li, K. Liu, J. Wang, W. Wang, X. Lu, Z. Tang, J. Lian, P. Zeng, Y. Wang and X. Zhan, Fused octacyclic electron acceptor isomers for organic solar cells, *J. Mater. Chem. A*, 2019, **7**, 21432-21437.

29. B. Kan, H. Feng, X. Wan, F. Liu, X. Ke, Y. Wang, Y. Wang, H. Zhang, C. Li, J. Hou and Y. Chen, Small-molecule acceptor based on the heptacyclic benzodi (cyclopentadithiophene) unit for highly efficient nonfullerene organic solar cells, *J. Am. Chem. Soc*, 2017, **139**, 4929-4934.

30. D. Raychev, O. Guskova, G. Seifert and J. U. Sommer, Conformational and electronic properties of small benzothiadiazole-cored oligomers with aryl flanking units: Thiophene versus Furan, *Comput. Mater. Sci.*, 2017, **126**, 287-298.

31. H. Lai, H. Chen, Y. Zhu, L. Chen, H.-H. Huang and F. He, An asymmetrical A–DAD–A-type acceptor simultaneously enhances voltage and current for efficient organic solar cells, *J. Mater. Chem. A*, 2020, **8**, 9670-9676.

32. Z. Luo, R. Ma, T. Liu, J. Yu, Y. Xiao, R. Sun, G. Xie, J. Yuan, Y. Chen, K. Chen, G. Chai, H. Sun, J. Min, J. Zhang, Y. Zou, C. Yang, X. Lu, F. Gao and H. Yan, Fine-tuning energy levels via asymmetric end groups enables polymer solar cells with efficiencies over 17%, *Joule*, 2020, **4**, 1236-1247.

33. J. Luke, E. M. Speller, A. Wadsworth, M. F. Wyatt, S. Dimitrov, H. K. H. Lee, Z. Li, W. C. Tsoi, I.

McCulloch, D. Bagnis, J. R. Durrant and J.-S. Kim, Twist and degrade-Impact of molecular structure on the photostability of nonfullerene acceptors and their photovoltaic blends, *Adv. Energy Mater.*, 2019, **9**, 1803755.

34. K. G. Jespersen, W. J. Beenken, Y. Zaushitsyn, A. Yartsev, M. Andersson, T. Pullerits and V. Sundstrom, The electronic states of polyfluorene copolymers with alternating donor-acceptor units, *J. Chem. Phys.*, 2004, **121**, 12613-12617.
35. S. Wood, J. Wade, M. Shahid, E. Collado-Fregoso, D. D. C. Bradley, J. R. Durrant, M. Heeney and J.-S. Kim, Natures of optical absorption transitions and excitation energy dependent photostability of diketopyrrolopyrrole (DPP)-based photovoltaic copolymers, *Energy Environ. Sci.*, 2015, **8**, 3222-3232.
36. Y. Chen, T. Liu, H. Hu, T. Ma, J. Y. L. Lai, J. Zhang, H. Ade and H. Yan, Modulation of end groups for low-bandgap nonfullerene acceptors enabling high‐performance organic solar cells, *Adv. Energy Mater.*, 2018, **8** 1801203.
37. S. Pang, R. Zhang, C. Duan, S. Zhang, X. Gu, X. Liu, F. Huang and Y. Cao, Alkyl chain length effects of polymer donors on the morphology and device performance of polymer solar cells with different acceptors, *Adv. Energy Mater.*, 2019, **9**, 1901740.
38. T. J. Aldrich, M. Matta, W. Zhu, S. M. Swick, C. L. Stern, G. C. Schatz, A. Facchetti, F. S. Melkonyan and T. J. Marks, *J. Am. Chem. Soc.*, Fluorination effects on indacenodithienothiophene acceptor packing and electronic structure, end-group redistribution, and solar cell photovoltaic response, 2019, **141**, 3274-3287.
39. S. M. Swick, J. M. Alzola, V. K. Sangwan, S. H. Amsterdam, W. Zhu, L. O. Jones, N. Powers−Riggs, A. Facchetti, K. L. Kohlstedt, G. C. Schatz, M. C. Hersam, M. R. Wasielewski and T.

J. Marks, Fluorinating π-extended molecular acceptors yields highly connected crystal structures and low reorganization energies for efficient solar cells, *Adv. Energy Mater.*, 2020, 10, 2000635.

40. H. Lai, Q. Zhao, Z. Chen, H. Chen, P. Chao, Y. Zhu, Y. Lang, N. Zhen, D. Mo, Y. Zhang, and F. He, Trifluoromethylation enables a 3d interpenetrated low-band-gap acceptor for efficient organic solar cells, *Joule*, 2020, **4**, 688-700.
41. H. Lai, H. Chen, J. Zhou, J. Qu, P. Chao, T. Liu, X. Chang, N. Zheng, Z. Xie and F. He, Isomer-free: precise positioning of chlorine-induced interpenetrating charge transfer for elevated solar conversion, *iScience*, 2019, **17**, 302-314.
42. J. Zhu, Y. Xiao, J. Wang, K. Liu, H. Jiang, Y. Lin, X. Lu and X. Zhan, Alkoxy-induced near-infrared sensitive electron acceptor for high-performance organic solar cells, *Chem. Mater.*, 2018, **30**, 4150-4156.
43. D. He, F. Zhao, J. Xin, J. J. Rech, Z. Wei, W. Ma, W. You, B. Li, L. Jiang, Y. Li and C. Wang, A fused ring electron acceptor with decacyclic core enables over 13.5% efficiency for organic solar cells, *Adv. Energy Mater.*, 2018, **8**, 1802050.
44. H. Lai, H. Chen, J. Zhou, J. Qu, M. Wang, W. Xie, Z. Xie and F. He, 3D interpenetrating network for high-performance nonfullerene acceptors via asymmetric chlorine substitution, *J. Phys. Chem. Lett.*, 2019, **10**, 4737-4743.
45. G. Zhang, X. K. Chen, J. Xiao, P. C. Y. Chow, M. Ren, G. Kupgan, X. Jiao, C. C. S. Chan, X. Du, R. Xia, Z. Chen, J. Yuan, Y. Zhang, S. Zhang, Y. Liu, Y. Zou, H. Yan, K. S. Wong, V. Coropceanu, N. Li, C. J. Brabec, J. L. Bredas, H. L. Yip and Y. Cao, Delocalization of exciton and electron wavefunction in non-fullerene acceptor molecules enables efficient organic solar cells, *Nat. Commun.* 2020, **11**, 3943.

46. W. Gao, M. Zhang, T. Liu, R. Ming, Q. An, K. Wu, D. Xie, Z. Luo, C. Zhong, F. Liu, F. Zhang, H. Yan and C. Yang, asymmetrical ladder-type donor-induced polar small molecule acceptor to promote fill factors approaching 77% for high-performance nonfullerene polymer solar cells, *Adv. Mater.*, 2018, 30, 1800052.

47. J. Song, X. Xue, B. Fan, L. Huo and Y. Sun, A novel bifunctional A-D-A type small molecule for efficient organic solar cells, *Mater. Chem. Front*., 2018,2, 1626-1630

48. J. Qu, Q. Zhao, J. Zhou, H. Lai, T. Liu, D. Li, W. Chen, Z. Xie and F. He, Multiple fused ring-based near-infrared nonfullerene acceptors with an interpenetrated charge-transfer network, *Chem. Mater.*, 2019, **31**, 1664-1671.

49. Q. Zhang, Q. Liang, D. K. Nandakumar, S. K. Ravi, H. Qu, L. Suresh, X. Zhang, Y. Zhang, L. Yang, A. T. S. Wee and S. C. Tan, Energy harvesting from shadow-effect, *Energy Environ. Sci*., 2020, **13**, 2404-2413.

50. J. V. Vaghasiya, K. K.Sonigara, L. Suresh, M. P. Fard, S. S. Soni, S. C. Tan, Efficient power generating devices utilizing low intensity indoor lights via non-radiative energy transfer mechanism from organic ionic redox couples, *Nano Energy*, 2019, 60, 457-466.

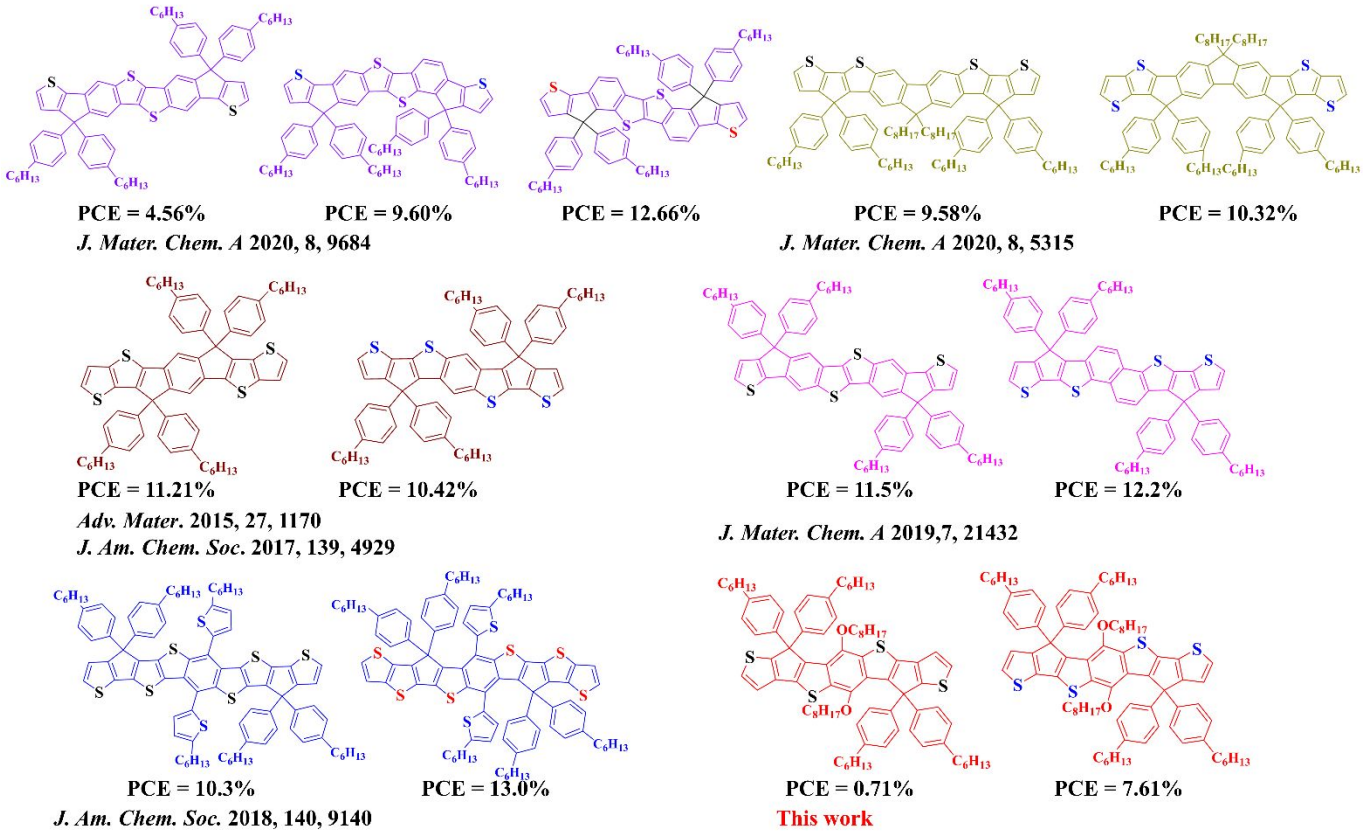

Figure 1. The isomeric core modifications of non-fullerene acceptors.

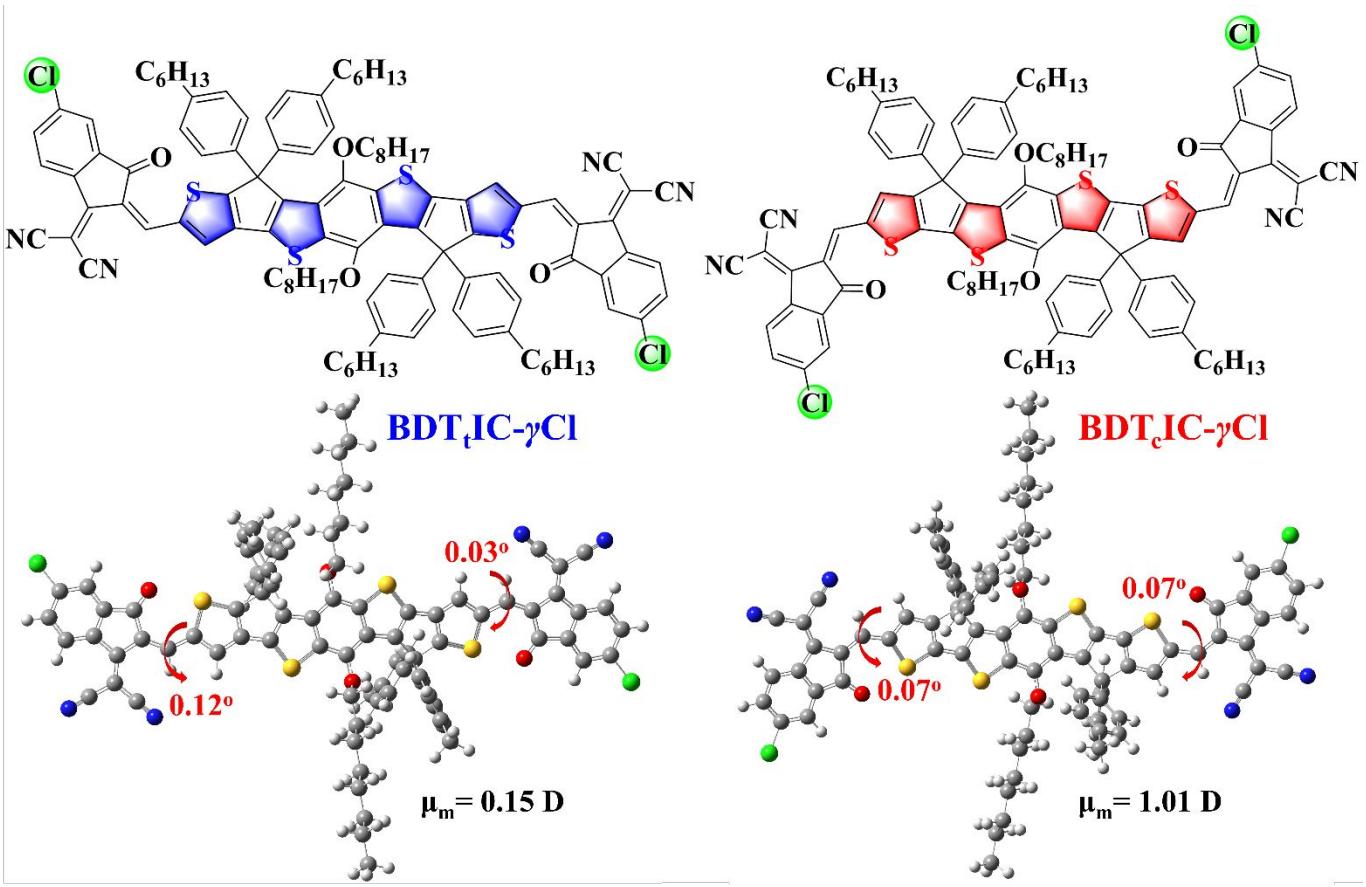

Figure 2. The structures of **BDT$_t$IC-γCl** and **BDT$_c$IC-γCl** and their configurations by DFT theoretical calculations.

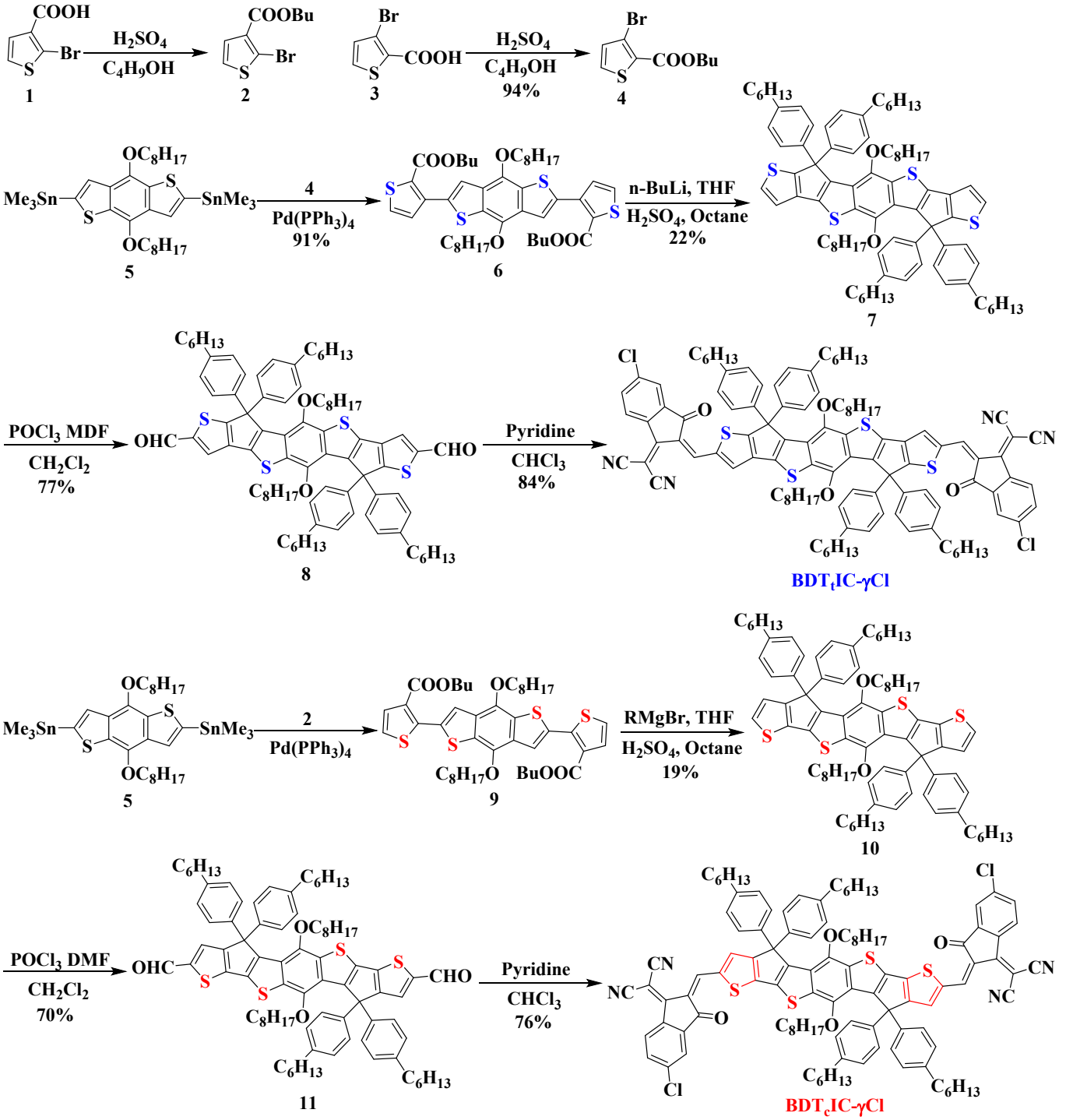

Scheme 1. The synthetic routes to **BDT_tIC-γCl** and **BDT_cIC-γCl**.

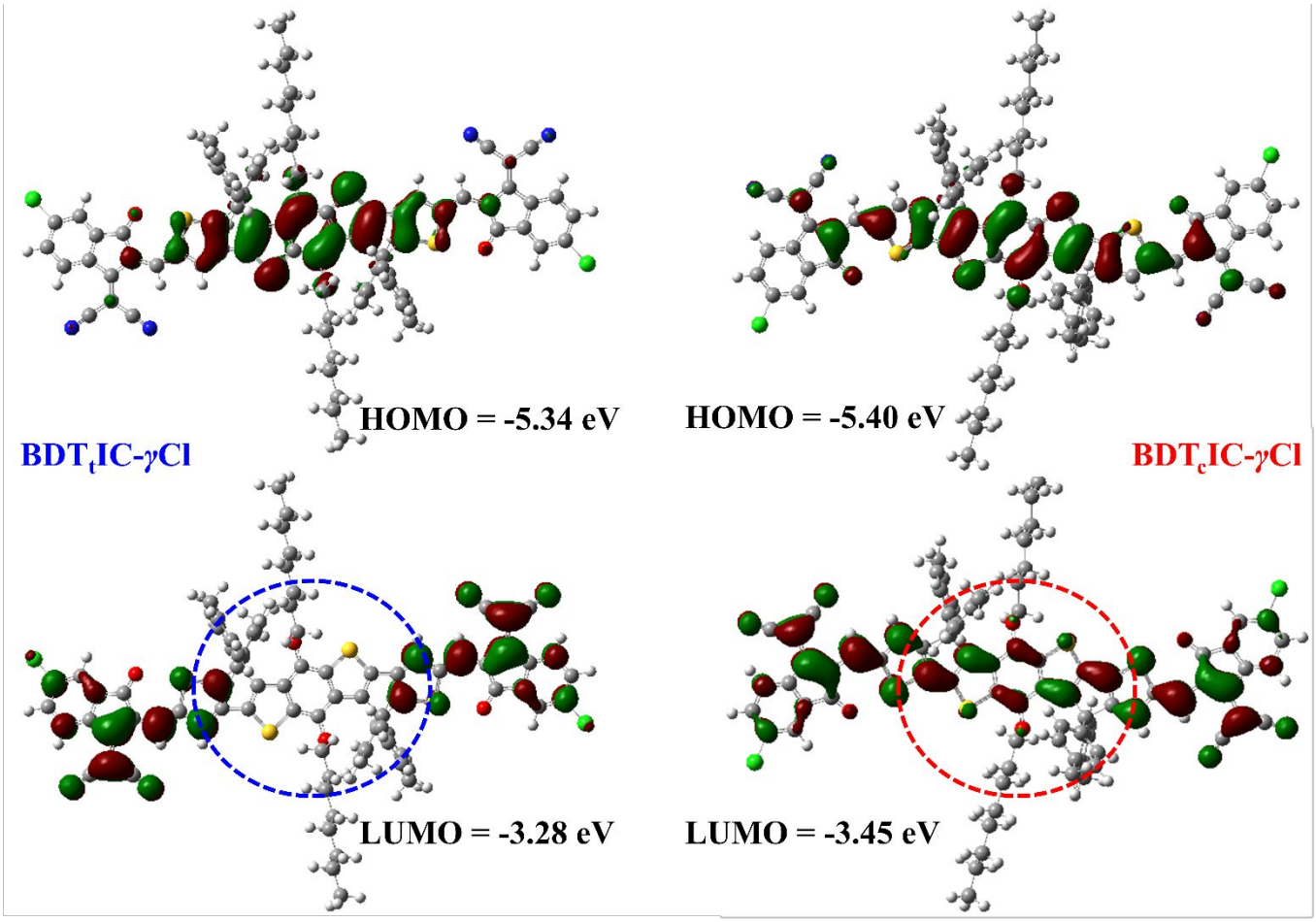

Figure 3. The electronic cloud distribution and corresponding energy levels of **BDT$_t$IC-γCl** and **BDT$_c$IC-γCl** by DFT theoretical calculations.

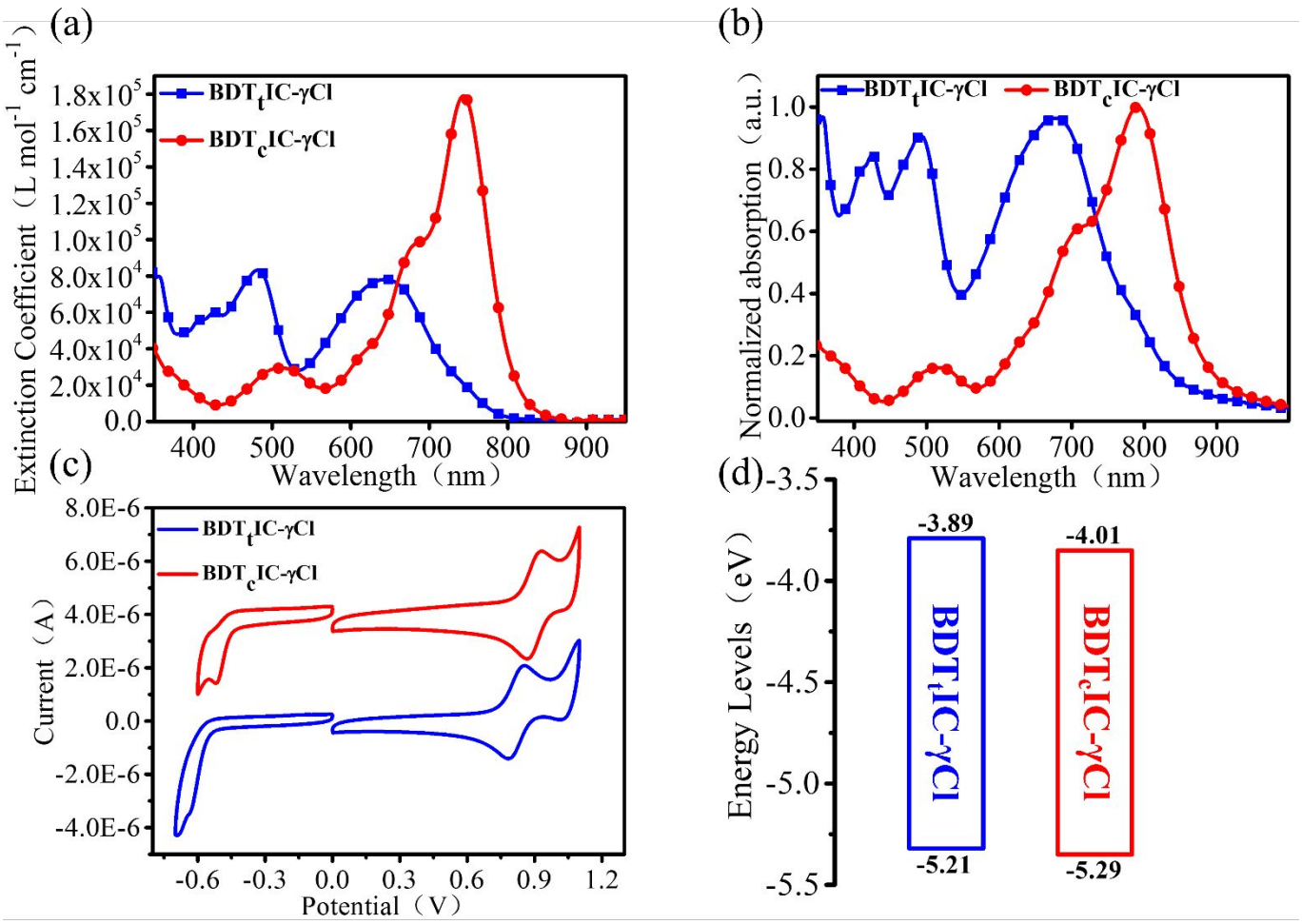

Figure 4. (a) The solution absorption (b) The films absorption (c) The electrochemical curves (d) The energy levels of **BDT_tIC-γCl** and **BDT_cIC-γCl**.

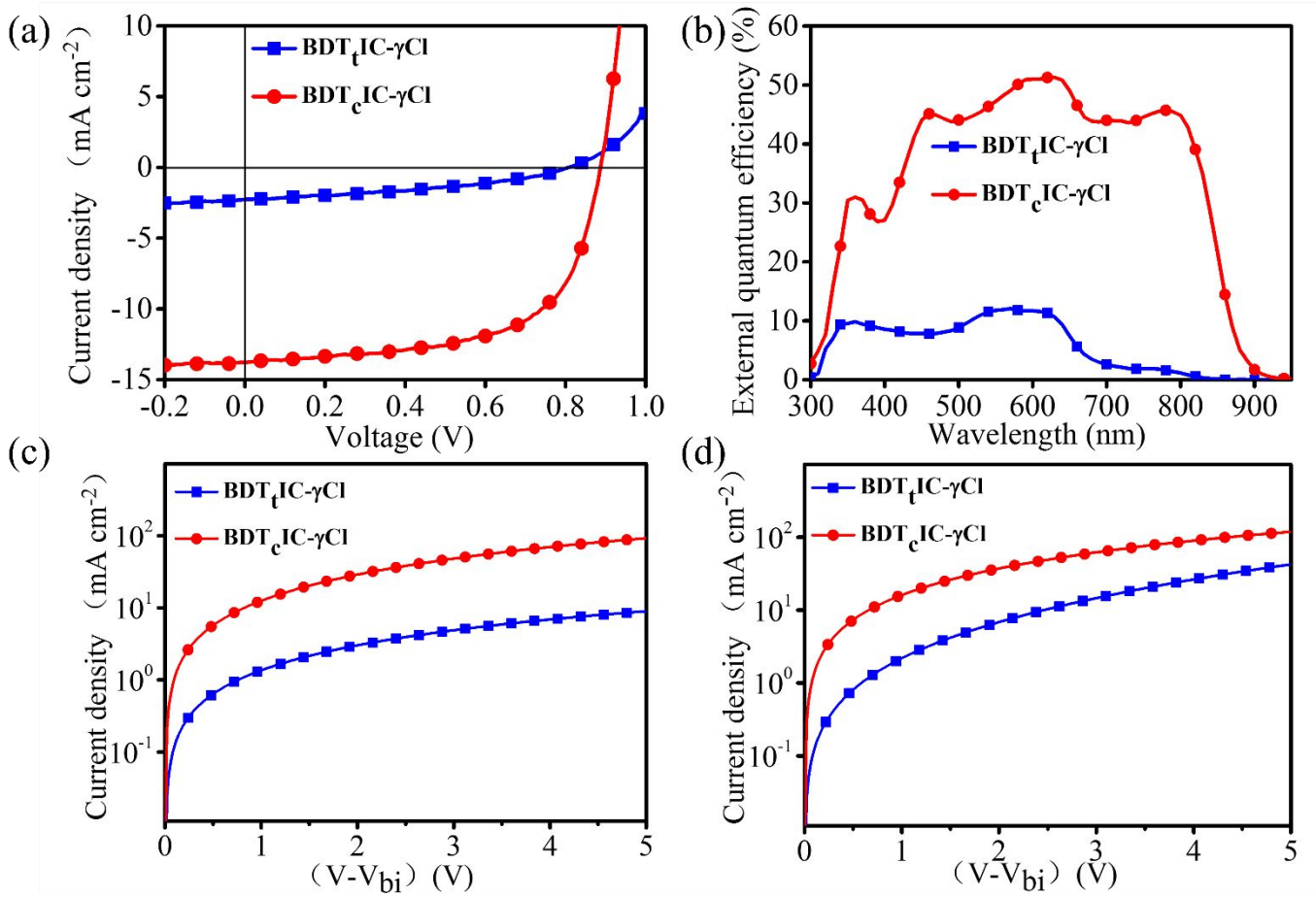

Figure 5. (a) The *J-V* curves (b) the EQE curves (c) electron mobilities and (d) hole mobilities of **BDT_tIC-γCl** and **BDT_cIC-γCl**.

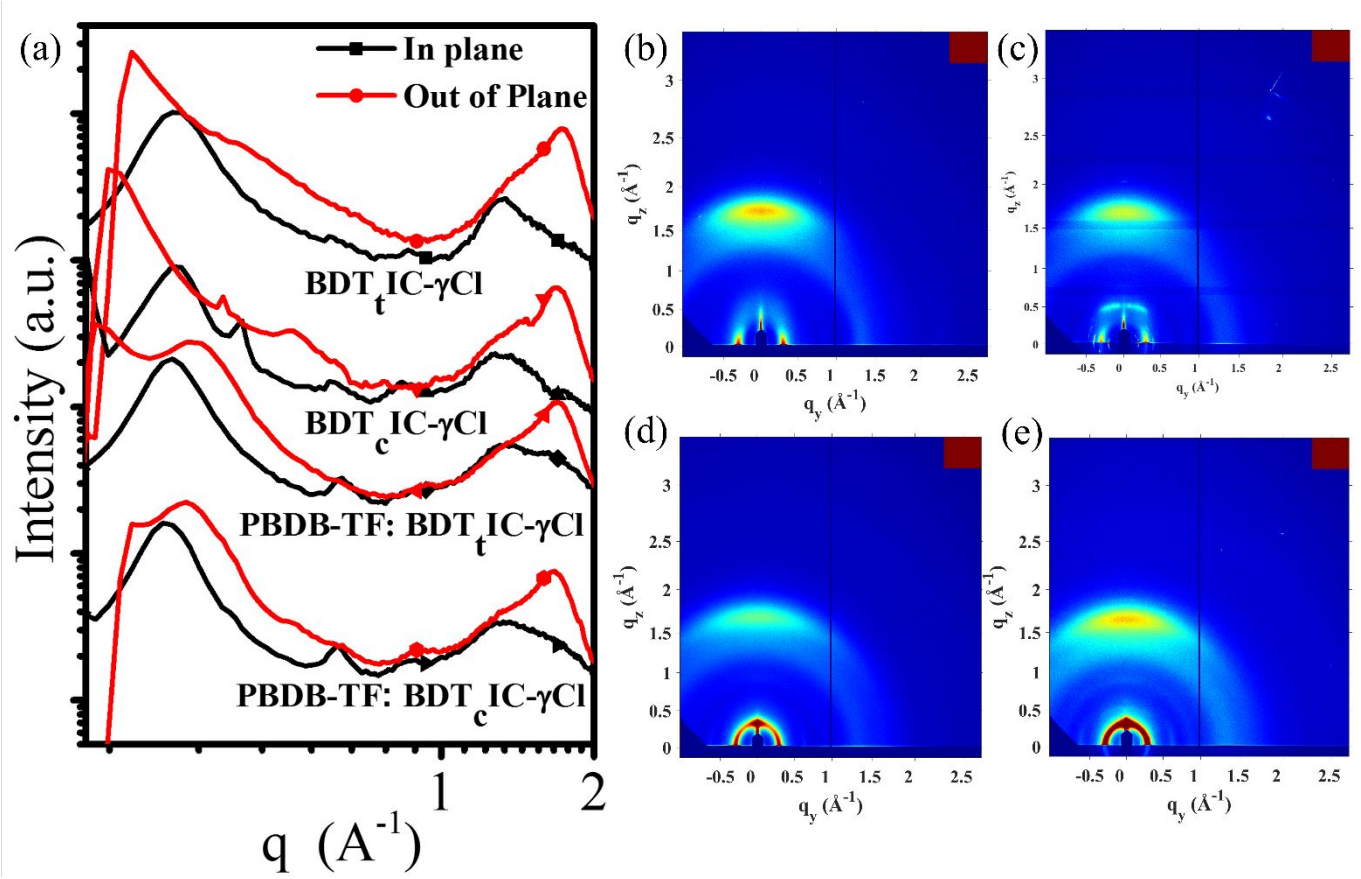

Figure 6. GIWAXS (a) line-cuts of in-plane and out-of-plane and the corresponding images of two acceptor-based neat films and blend films (b) **BDT$_t$IC-*γ*Cl** neat film, (c) **BDT$_c$IC-*γ*Cl** neat film, (d) **BDT$_t$IC-*γ*Cl** blend film, (e) **BDT$_c$IC-*γ*Cl** blend film.